

Towards the practical realization of high-performance Ag_2Se -based thermoelectric coolers

Feng Jiang, Zhengtao Wang, Wen Zhong, Yifan Zhou, Zhengyang Zhou, Longzhi Wu, Jiang Chen, Yao Xu, Xiaodong Wang, Feng Cao, Qian Zhang & Jun Mao

To cite this article: Feng Jiang, Zhengtao Wang, Wen Zhong, Yifan Zhou, Zhengyang Zhou, Longzhi Wu, Jiang Chen, Yao Xu, Xiaodong Wang, Feng Cao, Qian Zhang & Jun Mao (12 Mar 2026): Towards the practical realization of high-performance Ag_2Se -based thermoelectric coolers, Science and Technology of Advanced Materials, DOI: [10.1080/14686996.2026.2641882](https://doi.org/10.1080/14686996.2026.2641882)

To link to this article: <https://doi.org/10.1080/14686996.2026.2641882>



© 2026 The Author(s). Published by National Institute for Materials Science in partnership with Taylor & Francis Group.



View supplementary material [↗](#)



Accepted author version posted online: 12 Mar 2026.



Submit your article to this journal [↗](#)



View related articles [↗](#)



View Crossmark data [↗](#)

Publisher: Taylor & Francis & The Author(s). Published by National Institute for Materials Science in partnership with Taylor & Francis Group.

Journal: *Science and Technology of Advanced Materials*

DOI: 10.1080/14686996.2026.2641882

Towards the practical realization of high-performance Ag₂Se-based thermoelectric coolers

Feng Jiang^{a†}, Zhengtao Wang^{a†}, Wen Zhong^a, Yifan Zhou^a, Zhengyang Zhou^a, Longzhi Wu^a, Jiang Chen^a, Yao Xu^a, Xiaodong Wang^{a,d}, Feng Cao^c, Qian Zhang^{a, b, e*}, and Jun Mao^{a, b, e*}

a School of Materials Science and Engineering, and Institute of Materials Genome & Big Data, Harbin Institute of Technology (Shenzhen), Shenzhen 518055, P.R. China.

b State Key Laboratory of Precision Welding & Joining of Materials and Structures, Harbin Institute of Technology, Harbin 150001, P.R. China.

c School of Science, Harbin Institute of Technology (Shenzhen), Shenzhen 518055, P.R. China.

d Institute of Special Environments Physical Sciences, Harbin Institute of Technology (Shenzhen), Shenzhen 518055, P.R. China.

e School of Materials Science and Engineering, Shenzhen Key Laboratory of New Materials Technology, Shenzhen 518055, P.R. China.

[†]These authors contributed equally to this work.

*Corresponding authors, email: zhangqf@hit.edu.cn; maojun@hit.edu.cn;

Ag₂Se-based materials with promising room-temperature thermoelectric performance and excellent mechanical properties have been known for decades. However, the fabrication of the Ag₂Se-based devices toward the practical application of electronic cooling has seldom been reported. Herein, the synthesis of Ag₂Se material with a diameter of 25.4 mm was achieved. The homogeneous elemental distribution and similar thermoelectric properties demonstrate the high uniformity of the Ag₂Se sample. In addition, ~90 Ag/Ag₂Se/Ag legs can be obtained from a single Ag₂Se plate, and the interfacial contact resistivity of the Ag/Ag₂Se varies from 0.8 to 3.1 $\mu\Omega\text{ cm}^2$. Four thermoelectric devices based on n-type Ag₂Se and p-type (Bi, Sb)₂Te₃ have been fabricated, and they achieve a cooling temperature difference of ~56 K at the hot-side temperature of 300 K, demonstrating the great potential of Ag₂Se material for cooling applications.

Keywords: Thermoelectric cooling; Ag₂Se; Compositional homogeneity

1. Introduction

Thermoelectric materials enabling the direct conversion between electricity and heat are crucial for heat harvesting and electronic refrigeration [1-3]. The performance of a thermoelectric device is strongly dependent on the properties of the materials, which is expressed by the dimensionless figure of merit, $zT = S^2T/\rho\kappa$, where S , ρ , T , and κ are the Seebeck coefficient, electrical resistivity, absolute temperature, and thermal conductivity, respectively [4-7]. Pursuing high zT values is essential for achieving a device with excellent performance.

For solid-state cooling applications, materials with high room-temperature zT values will be favored [8-11]. For example, Bi_2Te_3 -based alloys have long been employed for commercial thermoelectric cooling applications due to their excellent performance near room temperatures [12-14]. However, the low natural abundance of the Te element and the poor mechanical properties of Bi_2Te_3 -based materials have motivated the development of novel materials with high thermoelectric performance and superior mechanical properties.

Recently, $\text{Mg}_3\text{Sb}_{2-x}\text{Bi}_x$ -based materials have been developed and exhibit superior performance near room temperature [15-21] and excellent mechanical properties [22-26]. Moreover, thermoelectric devices with excellent cooling performance have been reported [27-33]. For example, a two-stage Mg_3Bi_2 -based device was developed, and achieved a cooling temperature difference of 106.7 K at the hot-side temperature of 350 K [34]. In addition, a miniaturized Mg_3Bi_2 -based cooler was also fabricated, a high cooling power density of 5.7 W cm^{-2} and a cooling speed of 65 K s^{-1} were achieved [35].

As another potential candidate, n-type Ag_2Se has long been known as a high-performance thermoelectric material with a zT value of ~ 0.9 at room temperature [36]. Recently, Ag_2Se -based thermoelectric devices have been successfully fabricated and have achieved high cooling performance [37-39]. To enable the practical application of Ag_2Se in electronic cooling, it is critical to ensure the homogeneity of Ag_2Se -based materials for the practical fabrication of Ag_2Se -based thermoelectric coolers. However, such studies have seldom been reported.

Herein, the fabrication of the Ag_2Se -based thermoelectric coolers has been realized. Ag_2Se materials were prepared through ball-milling and sintering. In addition, a total of ~ 90 $\text{Ag}/\text{Ag}_2\text{Se}/\text{Ag}$ legs can be obtained from one $\text{Ag}/\text{Ag}_2\text{Se}/\text{Ag}$

plate with a diameter of 25.4 mm. The as-prepared samples not only exhibit good homogeneity but also present promising thermoelectric performance. In addition, four thermoelectric cooler devices based on the n-type Ag_2Se and p-type $(\text{Bi}, \text{Sb})_2\text{Te}_3$ have been fabricated, and they show a maximum temperature difference of ~ 56 K and a cooling power density of 1.56 W cm^{-2} at the hot-side temperature of 300 K.

2. Experimental method

2.1. Sample synthesis

Ag_2Se samples were prepared by the mechanical alloying method. Silver (Ag rods, with a diameter of ~ 1.9 mm and a length of ~ 5.1 mm, ZNXC, 99.995%) and selenium (Se shots, with a diameter of ~ 2.1 mm, ZNXC, 99.999%) were weighed in total 50 g according to the nominal composition of $\text{Ag}_2\text{Se}_{1.01}$ and loaded into a stainless jar with two stainless balls (with a diameter of ~ 12.6 mm and a mass of 15.9 g) in a high vacuum glove box (with both oxygen and water level below 1 ppm). The mixed raw materials were ball-milled in a high-energy ball milling machine (SPEX 8000M) for 8h (Once every 4 hours, with a 15-minute interval). The powders were then loaded in the graphite dies with a diameter of 10 mm, 12.7 mm, 20.0 mm, and 25.4 mm for densification at 523 K for 5 min using a spark plasma sintering under a pressure of 40 MPa (with a vacuum level of ~ 40 ppm).

2.2. Composition and microstructure characterization

The phase composition of the Ag_2Se samples was examined by X-ray diffraction (XRD) with $\text{Cu } K_\alpha$ radiation (Rigaku D/Max-2500 PC). The microstructure and surface morphology of the Ag_2Se sample, as well as the interfacial morphology of the Ag_2Se legs, were investigated by the scanning electron microscope (SEM, crossbeam 350) equipped with energy dispersive X-ray spectroscopy (EDS). The chemical composition of the Ag_2Se sample with a diameter of 25.4 mm was evaluated by the electron probe microanalysis (EPMA, JOEL, JXA-8100) with a voltage of 20.0 kV.

2.3. Thermoelectric properties characterization

The Ag_2Se samples with different diameters were cut into bar-shaped samples with dimensions of about $2 \text{ mm} \times 2 \text{ mm} \times 10 \text{ mm}$ for simultaneously measuring the electrical resistivity and Seebeck coefficient from 300 to 380 K on a commercial

apparatus (CTA-3, Cryoall) under a helium atmosphere. The Ag_2Se samples were cut into disks with dimensions of about $6 \text{ mm} \times 6 \text{ mm} \times 1 \text{ mm}$ for the measurement of thermal diffusivity (LFA 457, Netzsch) from 300 to 380 K. The specific heat capacity of Ag_2Se was measured by a differential scanning calorimeter (DSC 404F3, Netzsch) with an uncertainty of 3%, and the results are shown in Figure S1 (Supplementary Information). The density of the sample was measured by the Archimedean method. Eventually, the thermal conductivity is calculated by the product of thermal diffusivity, specific heat capacity, and sample density. The temperature-dependent Hall coefficients (R_H) were measured using the van der Pauw method and a four-probe configuration under a reversible magnetic field of 1.5 T and an electrical current of 150 mA from 300 to 380 K. The Hall carrier concentration (n_H) and Hall mobility (μ_H) were calculated based on the following relationships $n_H = 1/(eR_H)$ and $\mu_H = R_H/\rho$, respectively.

2.4. Thermoelectric cooler fabrication and performance characterization

Silver was used as the contact layer for Ag_2Se -based thermoelectric coolers. The Ag_2Se plate was loaded into a graphite die with a diameter of 25.4 mm, with 1.0 g Ag powder placed on each side within the glove box. The Ag/ Ag_2Se /Ag joint was prepared by using the spark plasma sintering at 523 K under a pressure of 40 MPa for 5 min. Importantly, an additional pressure of 10 MPa was maintained during the cooling process to ensure good contact property [38]. The commercial p-type $(\text{Bi}, \text{Sb})_2\text{Te}_3$ (RusTec LLC) was electroplated with Ni and applied as the p-type thermoelectric material. The thermoelectric cooler, consisting of 7 pairs of n-type Ag_2Se and p-type $(\text{Bi}, \text{Sb})_2\text{Te}_3$ legs, was assembled with the ceramic substrate that has been precoated with Cu and Ni layers, and with SnBi solder ($\text{Sn}_{42}\text{Bi}_{58}$, melting point 411 K). Then the assembly was subjected to reflow soldering at 458 K for 50 s with an external load. The contact electrical resistivity of the joints was measured using a homemade apparatus with alternating electrical currents [40].

The thermoelectric cooling performance of the Ag_2Se -based device was measured by a homemade apparatus in a vacuum [41]. The cooling power (Q_c) was evaluated by a reference sample with known thermal conductivity by using four thermocouples based on the one-dimensional Fourier heat conduction law.

$$Q_c = -\kappa A \frac{dT}{dz} \quad (1)$$

where κ and A are the thermal conductivity and the cross-sectional area of the reference sample, respectively. The cooling coefficient of performance (COP) is defined as the ratio of the Q_c and the input electrical power (P).

$$\text{COP} = Q_c / P \quad (2)$$

The temperature differences (ΔT) across the thermoelectric cooler under various currents were obtained under a steady condition that the hot-side temperature varies within 0.15 K in 60 s by subtracting the cold-side temperature (T_c) from the hot-side temperature (T_h), both measured with attached thermocouples [41]. The operational stability of the Ag_2Se -based thermoelectric coolers is evaluated by cycling tests with alternating currents between 1 A and 6 A. At each current, the test duration was set to 40 s, and the cooling temperature differences at 1 A and 6 A were recorded.

2.5. Simulation of the cooling performance of the Ag_2Se -based cooler

The cooling performance of the Ag_2Se -based thermoelectric cooler was simulated by finite element analysis software (COMSOL Multiphysics) based on the thermoelectric properties of the n-type Ag_2Se and the p-type $(\text{Bi}, \text{Sb})_2\text{Te}_3$. The simulation parameters are presented in Table S1, Supplementary Information. The thickness of the contact layer for Ag_2Se and $(\text{Bi}, \text{Sb})_2\text{Te}_3$ is set as 200 μm and 10 μm , respectively.

3. Results and Discussion

In order to evaluate the homogeneity of the chemical composition of Ag_2Se -based materials, different sizes of Ag_2Se were prepared, and the optical images are shown in Figure 1(a). All samples possess a distinct metallic luster and a high densification with a relative density of ~98% (Table S2, Supplementary Information). The X-ray diffraction patterns presented in Figure 1(b) indicated that the prepared Ag_2Se materials with different sizes show a single phase with an orthorhombic structure, which is indexed as PDF#24-1041. The full width at half maximum (FWHM) of the Ag_2Se sample with a diameter of 25.4 mm ($\phi 25.4$) is 0.2° , further demonstrating good crystallinity. To further evaluate the uniformity of the $\phi 25.4$ sample, elemental distribution and chemical composition are characterized, and the results are shown in Figure 1(c) and Figure 1(d). The elements are distributed homogeneously without

obvious elemental segregations in this sample, as shown in Figure 1(c) and Figure S2 (Supplementary Information). The electron probe microanalysis results presented in Figure 1(d) show a highly uniform distribution of chemical composition in the different regions. The measured composition of the sample is $\text{Ag}_2\text{Se}_{0.93}$, which is close to the reported values [42].

To evaluate the homogeneity of thermoelectric properties, five bar-shaped and five disk-shaped specimens were prepared for measuring electrical properties and thermal conductivity, respectively. As shown in Figure 2(a), the electrical resistivities of Ag_2Se show a monotonic decrease from $\sim 9.3 \mu\Omega \text{ m}$ at 300 K to $\sim 7.5 \mu\Omega \text{ m}$ at 380 K. As a narrow bandgap semiconductor [43-45], the bipolar effect induces excitation of minor carriers with the elevation of temperature, leading to an increase in carrier concentration (Figure S3, Supplementary Information) [46, 47]. Simultaneously, the Seebeck coefficient exhibited a similar trend with the electrical resistivity as shown in Figure 2(b). The negative Seebeck coefficients of Ag_2Se indicate n-type semiconductor behavior, which is likely attributed to the intrinsic Se vacancy [48, 49]. The Seebeck coefficient of Ag_2Se decreases with the increase of temperature from $-153 \mu\text{V K}^{-1}$ at 300 K to $-145 \mu\text{V K}^{-1}$ at 380 K, further supporting the onset of bipolar effect. As shown in Figure 2(c), the power factor ($PF = S^2/\rho$) of Ag_2Se shows a slight increase from $\sim 25 \mu\text{W cm}^{-1} \text{ K}^{-2}$ at 300 K to $\sim 28 \mu\text{W cm}^{-1} \text{ K}^{-2}$ at 380 K. Figure 2(d) shows the temperature-dependent thermal conductivity of Ag_2Se . The total thermal conductivity shows a continuous increase from $\sim 0.95 \text{ W m}^{-1} \text{ K}^{-1}$ at 300 K to $\sim 1.15 \text{ W m}^{-1} \text{ K}^{-1}$ at 380 K. The total thermal conductivity is composed of the lattice thermal conductivity (κ_L), the electronic thermal conductivity (κ_e), and the bipolar thermal conductivity (κ_{bip}). Due to the bipolar conduction, the enhanced total thermal conductivity should be ascribed to the increased electronic thermal conductivity [50, 51] ($\kappa_e = L\sigma T$, where L is the Lorenz number, calculated by the empirical formula, $L = 1.5 + \exp(|S|/115)$ [52]), and the additional contribution from the bipolar thermal conductivity, as shown in Figure 2(e) and Figure S4, Supplementary Information. Finally, the zT values of Ag_2Se -based materials are around 0.8 at 300 K, and the average zT (zT_{avg}) is ~ 0.85 at the temperature range from 300 to 380 K, as shown in Figure 2(f). The overall thermoelectric properties of five Ag_2Se samples are comparable (Figure S5, Supplementary Information). These results demonstrate the homogeneous chemical composition and promising thermoelectric performance of the prepared Ag_2Se sample.

To fabricate the Ag₂Se-based thermoelectric coolers, the preparation of the Ag/Ag₂Se/Ag joint was realized by spark plasma sintering, and a residual pressure was maintained during the cooling process to minimize the detrimental effect of phase transition [38]. As depicted in the inset of Figure 3(a), ~90 Ag₂Se-based legs with dimensions of 1.8 mm × 1.8 mm × 2.6 mm were obtained through cutting a single ϕ 25.4 mm Ag/Ag₂Se/Ag plate [53]. To evaluate the electrical contact resistivity at the Ag/Ag₂Se/Ag interface, five Ag₂Se legs were characterized, as shown in Figure 3(a). The contact resistivity of the Ag/Ag₂Se interface varies from 0.8 to 3.1 $\mu\Omega\text{ cm}^2$, indicating negligible electrical parasitic loss. To be noted that the contact resistivity is lower than that of Ni/Ag₂Se (ρ_c of ~12 $\mu\Omega\text{ cm}^2$) [37], and comparable with our previous result (ρ_c of ~2.9 $\mu\Omega\text{ cm}^2$) [38]. The Ag₂Se-based legs were further bonded with the Cu electrode (deposited with a thin Ni layer) by using the SnBi solder at 458 K. Scanning electron microscopy and energy dispersive spectroscopy were applied to characterize the interface of the soldered joint. Figure 3(b) shows clear and distinct boundaries between the successive layers: Cu electrode/SnBi solder, SnBi solder/Ag contact layer, and Ag contact layer/Ag₂Se. The contact resistivity of the soldered Ag/Ag₂Se joint is 1.5 $\mu\Omega\text{ cm}^2$ (Figure S6, Supplementary Information), indicating a good contact property. In addition, the corresponding energy dispersive spectroscopy mapping results (Figure 3(c-h)) reveal the homogeneous elemental distributions without obvious diffusions. Furthermore, the linear EDS scanning across the Ag/Ag₂Se joint illustrates the distinct interfaces. (Figure S7, Supplementary Information). In addition, there is a narrow diffusion layer between Ag/SnBi boundary, which is beneficial to ensure a good bonding strength (Figure S8, Supplementary Information). The above results confirm that Ag is a good contact layer for Ag₂Se and the feasibility for the practical fabrication of Ag₂Se-based thermoelectric coolers.

To further validate the thermoelectric performance of the Ag₂Se sample, a cooling device based on 7 pairs of n-type Ag₂Se and p-type (Bi, Sb)₂Te₃ was fabricated. The cooling performance of the Ag₂Se-based device was characterized on a homemade apparatus at the hot-side temperature of 300 K. As shown in Figure 4(a), there is a good linear relationship between the cooling power and cooling temperature difference of the Ag₂Se-based device. When the applied electrical current was 7 A, the device achieved a maximum cooling power of ~2.46 W, corresponding to a cooling power density of 1.46 W cm⁻². In addition, at the optimal electrical current, the maximum cooling temperature difference is 55.4 K, which is comparable to the

previously reported Ag_2Se -based coolers [37-39], and lower than Bi_2Te_3 -based [14, 54] and $\text{Mg}_3(\text{Sb, Bi})_2$ -based devices [30, 32, 34] (Table S3, Supplementary Information). The relationship between cooling power and electrical current under different cooling temperature differences is presented in Figure 4(b). Correspondingly, the steady-state cooling performance of the Ag_2Se -based device is simulated, and the impact of thermal radiation is considered (Figure S9, Supplementary Information). The cooling power experiences an increment with the increase in electrical current from 1 to 7 A. In addition, the Ag_2Se -based device also achieved a maximum cooling power of 2.76 W and a maximum cooling temperature difference of 61.2 K at the hot-side temperature of 325 K (Figure S10-11, Supplementary Information). The cooling coefficient of performance of the Ag_2Se -based device exhibits a nearly linear relationship with the cooling temperature difference, as shown in Figure 4(c). The inset image shows the side view of the Ag_2Se -based cooler. The coefficient of performance decreases with the increase in cooling temperature difference. Recently, a criterion for evaluating the measurement uncertainty has been proposed: the coefficient of performance should be 0.5 at the optimum electrical current, under the condition of maximum cooling power and zero cooling temperature difference [55]. Herein, the Ag_2Se -based device achieved a coefficient of performance of 0.504 at the zero temperature difference and the optimal electrical current of 7 A (Figure S12, Supplementary Information), further supporting the reliability of the thermoelectric cooling performance measurement.

To evaluate the reproducibility of their cooling performance, four Ag_2Se -based thermoelectric coolers were fabricated and characterized. The cooling temperature differences as a function of electrical current at the hot-side temperatures of 300 K are presented in Figure 4(d). The inset of Figure 4(d) shows the optical image of four Ag_2Se -based devices. It is clear that the cooling temperature difference increases with the increase in electrical current, and reaches a maximum value of ~56 K at the optimal electrical current for four devices. In addition, the operational stability of the Ag_2Se -based device is also investigated with cycling tests between the electrical currents of 1 A and 6 A at the hot-side temperature of 300 K, and the results are shown in Figure 4(e). It can be noted that the cooling temperature difference at two electrical currents experiences a fluctuation within 2% after more than 2000 cycles. Furthermore, the interface of the Ag_2Se -based thermoelectric cooler after the cycling is also characterized, as shown in Figure S13 (Supplementary Information). It can be

noted that there is a clear boundary between the various interfaces without obvious elemental diffusions, demonstrating a superior stability of the Ag₂Se-based thermoelectric cooler.

4. Conclusion

Herein, the fabrication of the Ag₂Se-based thermoelectric coolers has been realized. Good compositional homogeneity and excellent thermoelectric performance have been achieved in the ϕ 25.4 mm Ag₂Se sample. Using the spark plasma sintering, the Ag/Ag₂Se/Ag joint is prepared, and a total amount of ~90 Ag/Ag₂Se/Ag legs can be obtained with a low contact resistivity ranging from 0.8 to 3.1 $\mu\Omega\text{ cm}^2$. Four thermoelectric devices based on the n-type Ag₂Se and p-type (Bi, Sb)₂Te₃ have been fabricated, and they show a maximum cooling temperature difference of ~56 K at the hot-side temperature of 300 K. In addition, it also shows excellent operational stability after more than 2000 cycles of electrical currents between 1 A and 6 A. Our results demonstrate that Ag₂Se-based materials and devices hold great promise for practical applications of electronic refrigeration.

Acknowledgments

The authors acknowledge the support from Shang Gao for SEM characterization.

Disclosure statement

No potential conflict of interest was reported by the authors.

Conflict of Interest

The authors declare no conflict of interest.

Fundings

This work was supported by the National Natural Science Foundation of China for Distinguished Young Scholars (52425108), the Shenzhen Science and Technology Program (KQTD20200820113045081 and SYSPG20241211173609003), and the GuangDong Basic and Applied Basic Research Foundation (2024B1515040022). J.M. acknowledges the financial support from the National Natural Science Foundation of China (52473298) and the Shenzhen Science and Technology Program (RCJC20221008092725020). Q.Z. acknowledges the financial support from the

National Natural Science Foundation of China (52172194), and the Shenzhen Science and Technology Program (RCJC20210609103733073, JCYJ20241202123659001). F.C. acknowledges the financial support from the National Natural Science Foundation of China (52472196). F.J. acknowledges the financial support from the National Natural Science Foundation of China (12504050), the Shenzhen Excellent Science and Technology Innovation Talent Training Program (RCBS20231211090701009).

ORCID

Feng Jiang, <https://orcid.org/0000-0002-1220-7194>

Xiaodong Wang, <https://orcid.org/0009-0006-4718-6705>

Feng Cao, <https://orcid.org/0000-0003-3140-4502>

Qian Zhang, <https://orcid.org/0000-0001-5975-9781>

Jun Mao, <https://orcid.org/0000-0001-5275-8954>

Author Contributions

J.M., Q.Z., and F.J. conceived the idea, F.J. prepared the Ag₂Se sample and performed the thermoelectric properties measurement, F.J., J.C., and Y.X. performed the characterizations, Y.F.Z., and Z.Y.Z. performed the Hall measurement, W.Z., F.J., and Z.T.W. fabricated the Ag₂Se-based device, and F.J., L.Z.W., and Z.T.W. performed the thermoelectric cooling performance measurement, F.J., J.M., X.D.W., and F.C. analyzed the data, J.M., F.J., and Q.Z. wrote and edited the manuscript, and everyone reviewed and revised it. All authors contributed helpful discussions to this work.

References

- [1] Snyder GJ, Toberer ES. Complex thermoelectric materials. *Nat Mater.* (2008);7(2):105-114. doi: 10.1038/nmat2090
- [2] Mao J, Liu ZH, Zhou JW, et al. Advances in thermoelectrics. *Adv Phys.* (2018);67(2):69-147. doi: 10.1080/00018732.2018.1551715
- [3] Petsagkourakis I, Tybrandt K, Crispin X, et al. Thermoelectric materials and applications for energy harvesting power generation. *Sci Technol Adv Mater.* (2018);19(1):836-862. doi: 10.1080/14686996.2018.1530938
- [4] Liu WS, Hu JZ, Zhang SM, et al. New trends, strategies and opportunities in thermoelectric materials: A perspective. *Mater Today Phys.* (2017);1(1):50-60. doi: 10.1016/j.mtphys.2017.06.001
- [5] Zhu TJ, Liu YT, Fu CG, et al. Compromise and synergy in high-efficiency thermoelectric materials. *Adv Mater.* (2017);29(14):1605884. doi: 10.1002/adma.201605884
- [6] Yin L, Yang F, Bao X, et al. Low-temperature sintering of Ag nanoparticles for high-performance thermoelectric module design. *Nat Energy.* (2023);8(1):665-674. doi: 10.1038/s41560-023-01245-4
- [7] Jiang F, Xia C-L, Zhu Y-B, et al. Thermoelectric transport properties of p-type $\text{Bi}_2\text{Se}_3\text{-Sb}_2\text{Se}_3\text{-In}_2\text{Se}_3$ high entropy compounds. *Rare Met.* (2024);43(7):3415-3421. doi: 10.1007/s12598-024-02658-0
- [8] Pourkiaei SM, Ahmadi MH, Sadeghzadeh M, et al. Thermoelectric cooler and thermoelectric generator devices: A review of present and potential applications, modeling and materials. *Energy.* (2019);186(3):115849. doi: 10.1016/j.energy.2019.07.179
- [9] Mao J, Chen G, Ren ZF. Thermoelectric cooling materials. *Nat Mater.* (2021);20(4):454-461. doi: 10.1038/s41563-020-00852-w
- [10] Shi X-L, Li N-H, Li M, et al. Toward efficient thermoelectric materials and devices: Advances, challenges, and opportunities. *Chem Rev.* (2025);125(16):7525-7724. doi: 10.1021/acs.chemrev.5c00060
- [11] Liu S, Li AR, Hao XW, et al. Synthesis and thermal stability of topological semimetal RMnSb_2 (R = Yb, Sr, Ba, Eu). *Sci Technol Adv Mater.* (2025);26(1):2512702. doi: 10.1080/14686996.2025.2512702
- [12] Zhao DL, Tan G. A review of thermoelectric cooling: Materials, modeling and applications. *Appl Therm Eng.* (2014);66(1):15-24. doi: 10.1016/j.applthermaleng.2014.01.074
- [13] Wang XD, Cheng JX, Yin L, et al. Organic/inorganic hybrid design as a route for promoting the $\text{Bi}_{0.5}\text{Sb}_{1.5}\text{Te}_3$ for high-performance thermoelectric power generation. *Adv Funct Mater.* (2022);32(24):2200307. doi: 10.1002/adfm.202200307

- [14] Sun YX, Wu H, Dong XY, et al. High performance BiSbTe alloy for superior thermoelectric cooling. *Adv Funct Mater.* (2023);33(28):2301423. doi: 10.1002/adfm.202301423
- [15] Tamaki H, Sato HK, Kanno T. Isotropic Conduction Network and Defect Chemistry in $\text{Mg}_{3+\delta}\text{Sb}_2$ -Based Layered Zintl Compounds with High Thermoelectric Performance. *Adv Mater.* (2016);28(46):10182-10187. doi: 10.1002/adma.201603955
- [16] Zhang J, Song L, Pedersen SH, et al. Discovery of high-performance low-cost n-type Mg_3Sb_2 -based thermoelectric materials with multi-valley conduction bands. *Nat Commun.* (2017);8(3):13901. doi: 10.1038/ncomms13901
- [17] Mao J, Wu YX, Song SW, et al. Defect engineering for realizing High thermoelectric performance in n-type Mg_3Sb_2 -based materials. *ACS Energy Lett.* (2017);2(10):2245-2250. doi: 10.1021/acsenenergylett.7b00742
- [18] Shi XM, Zhao TT, Zhang XY, et al. Extraordinary n-type Mg_3SbBi thermoelectrics enabled by yttrium doping. *Adv Mater.* (2019);31(36):1903387. doi: 10.1002/adma.201903387
- [19] Shu R, Zhou YC, Wang Q, et al. $\text{Mg}_{3+\delta}\text{Sb}_x\text{Bi}_{2-x}$ family: A promising substitute for the state-of-the-art n-type thermoelectric materials near room temperature. *Adv Funct Mater.* (2019);29(4):1807235. doi: 10.1002/adfm.201807235
- [20] Imasato K, Kang SD, Snyder GJ. Exceptional thermoelectric performance in $\text{Mg}_3\text{Sb}_{0.6}\text{Bi}_{1.4}$ for low-grade waste heat recovery. *Energy Environ Sci.* (2019);12(3):965-971. doi: 10.1039/c8ee03374a
- [21] Jiang F, Wu XZ, Zhu YB, et al. Boosting room-temperature thermoelectric performance of $\text{Mg}_3\text{Sb}_{1.5}\text{Bi}_{0.5}$ material through breaking the contradiction between carrier concentration and carrier mobility. *Acta Mater.* (2024);265(10):119636. doi: 10.1016/j.actamat.2023.119636
- [22] Jiang F, Feng T, Zhu YB, et al. Extraordinary thermoelectric performance, thermal stability and mechanical properties of n-type $\text{Mg}_3\text{Sb}_{1.5}\text{Bi}_{0.5}$ through multi-dopants at interstitial site. *Mater Today Phys.* (2022);27(10):100835. doi: 10.1016/j.mtphys.2022.100835
- [23] Zhao P, Xue WH, Zhang Y, et al. Plasticity in single-crystalline Mg_3Bi_2 thermoelectric material. *Nature.* (2024);631(8022):777-782. doi: 10.1038/s41586-024-07621-8
- [24] Li AR, Wang YC, Li YZ, et al. High performance magnesium-based plastic semiconductors for flexible thermoelectrics. *Nat Commun.* (2024);15(1):5108. doi: 10.1038/s41467-024-49440-5
- [25] Zhang TY, Yan J, Ke J, et al. Substantial planar plastic anisotropy in inorganic Mg_3Bi_2 single crystals. *Proc Natl Acad Sci U S A.* (2025);122(47):2516449122. doi: 10.1073/pnas.2516449122
- [26] Hu MY, Yang JM, Wang Y, et al. Helical dislocation-driven plasticity and

flexible high-performance thermoelectric generator in α -Mg₃Bi₂ single crystals. Nat Commun. (2025);16(1):128. doi: 10.1038/s41467-024-55689-7

- [27] Mao J, Zhu HT, Ding ZW, et al. High thermoelectric cooling performance of n-type Mg₃Bi₂-based materials. Science. (2019);365(6452):495-498. doi: 10.1126/science.aax7792
- [28] Liu ZH, Gao Wh, Oshima H, et al. Maximizing the performance of n-type Mg₃Bi₂ based materials for room-temperature power generation and thermoelectric cooling. Nat Commun. (2022);13(1):1120. doi: 10.1038/s41467-022-28798-4
- [29] Ying PJ, Wilkens L, Reith H, et al. A robust thermoelectric module based on MgAgSb/Mg₃(Sb,Bi)₂ with a conversion efficiency of 8.5% and a maximum cooling of 72 K. Energy Environ Sci. (2022);15(6):2557-2566. doi: 10.1039/d2ee00883a
- [30] Xie LJ, Yang JW, Liu ZY, et al. Highly efficient thermoelectric cooling performance of ultrafine-grained and nanoporous materials. Mater Today. (2023);65(4):5-13. doi: 10.1016/j.mattod.2023.03.021
- [31] Bano S, Chetty R, Babu J, et al. Mg₃(Sb,Bi)₂-based materials and devices rivaling bismuth telluride for thermoelectric power generation and cooling. Device. (2024);2(7):100408. doi: 10.1016/j.device.2024.100408
- [32] Zhang XF, Zhu HT, Dong XJ, et al. High-performance MgAgSb/Mg₃(Sb,Bi)₂-based thermoelectrics with $\eta = 12\%$ at $T \leq 583\text{K}$. Joule. (2024);8(12):3324-3335. doi: 10.1016/j.joule.2024.08.013
- [33] Yang HY, Lin CH, Liang K, et al. High-performance double-stage Mg₃Bi₂-based thermoelectric cooler. Innov Mater. (2025);3(2):100130. doi: 10.59717/j.xinn-mater.2025.100130
- [34] Ma XJ, Lin CH, Yang HY, et al. Elevating thermoelectric performance in the sub-ambient temperature range for electronic refrigeration. Innovation. (2025);6(5):100864. doi: 10.1016/j.xinn.2025.100864
- [35] Lin CH, Ma XJ, Liang K, et al. Miniaturized Mg₃Bi₂-based thermoelectric cooler for localized electronic thermal management. Nat Commun. (2025);16(1):7779. doi: 10.1038/s41467-025-63174-y
- [36] Wu H, Shi X-L, Duan JG, et al. Advances in Ag₂Se-based thermoelectrics from materials to applications. Energy Environ Sci. (2023);16(5):1870-1906. doi: 10.1039/d3ee00378g
- [37] Liu M, Zhang XY, Zhang SX, et al. Ag₂Se as a tougher alternative to n-type Bi₂Te₃ thermoelectrics. Nat Commun. (2024);15(1):6580. doi: 10.1038/s41467-024-50898-6
- [38] Jiang F, Lin CH, Cheng JX, et al. Prefer-oriented Ag₂Se crystal for high-performance thermoelectric cooling. Adv Funct Mater. (2024);35(6):2415000. doi: 10.1002/adfm.202415000

- [39] Zhao SY, Shi XL, Zhou Q, et al. Substitution energy-guided screening of diffusion barrier materials for Ag₂Se-based thermoelectric coolers. *Nano Res.* (2025);18(10):94907903. doi: 10.26599/NR.2025.94907903
- [40] Sun Y, Yin L, Zhang ZW, et al. Low contact resistivity and excellent thermal stability of p-type YbMg_{0.8}Zn_{1.2}Sb₂/Fe-Sb junction for thermoelectric applications. *Acta Mater.* (2022);235(2):118066. doi: 10.1016/j.actamat.2022.118066
- [41] Liang K, Yang HY, Zhao P, et al. Characterizing the thermoelectric cooling performance across a broad temperature range. *Rev Sci Instrum.* (2023);94(10):105112. doi: 10.1063/5.0165551
- [42] Yang DW, Su XL, Meng FC, et al. Facile room temperature solventless synthesis of high thermoelectric performance Ag₂Se via a dissociative adsorption reaction. *J Mater Chem A.* (2017);5(44):23243-23251. doi: 10.1039/c7ta08726h
- [43] Taylor PF, Wood C. Thermoelectric properties of Ag₂Te and Ag₂Se. *Adv Energy Convers.* (1961);1(1):141-145. doi: 10.1016/0365-1789(61)90023-6
- [44] Dalven R, Gill R. Energy gap in β -Ag₂Se. *Phys Rev.* (1967);159(3):645-649. doi: 10.1103/PhysRev.159.645
- [45] Dalven R, Gill R. Electrical properties of β -Ag₂Te and β -Ag₂Se from 4.2° to 300°K. *J Appl Phys.* (1967);38(2):753-756. doi: 10.1063/1.1709406
- [46] Jin M, Liang JS, Qiu PF, et al. Investigation on low-temperature thermoelectric properties of Ag₂Se polycrystal fabricated by using zone-melting method. *J Phys Chem Lett.* (2021);12(34):8246-8255. doi: 10.1021/acs.jpcclett.1c02139
- [47] Qiu JM, Zhi SZ, Zhao P, et al. Revealing the significant role of band structure asymmetry on thermoelectric bipolar conduction. *Phys Rev B.* (2025);111(4):045203. doi: 10.1103/PhysRevB.111.045203
- [48] Ballikaya S, Oner Y, Temel T, et al. Thermoelectric and thermal stability improvements in nano-Cu₂Se included Ag₂Se. *J Solid State Chem.* (2019);273(122-127. doi: 10.1016/j.jssc.2019.02.037
- [49] Jiang F, Xia CL, Zhu YB, et al. Thermoelectric properties of p-type polycrystalline Bi_{0.8}Sb_{0.8}In_{0.4}Se₃. *Appl Phys Lett.* (2021);118(19):193903. doi: 10.1063/5.0050604
- [50] Mi WL, Qiu PF, Zhang TS, et al. Thermoelectric transport of Se-rich Ag₂Se in normal phases and phase transitions. *Appl Phys Lett.* (2014);104(13):133903. doi: 10.1063/1.4870509
- [51] Ye S, Zhi SZ, Ma XJ, et al. Superior electron transport in the single-crystalline TiCoSb-based half-Heuslers. *Nat Commun.* (2025);16(1):1812. doi: 10.1038/s41467-025-56961-0
- [52] Kim H-S, Gibbs ZM, Tang YL, et al. Characterization of Lorenz number with

Seebeck coefficient measurement. *APL Mater.* (2015);3(4):041506. doi: 10.1063/1.4908244

- [53] Wang HY, Liu XF, Zhou ZZ, et al. Constructing n-type $\text{Ag}_2\text{Se}/\text{CNTs}$ composites toward synergistically enhanced thermoelectric and mechanical performance. *Acta Mater.* (2022);223(3):117502. doi: 10.1016/j.actamat.2021.117502
- [54] Zhang Y, Xu G, Nozariasbmarz A, et al. Thermoelectric cooling performance enhancement in BiSeTe alloy by microstructure modulation via hot extrusion. *Small Sci.* (2023);4(2):2300245. doi: 10.1002/smssc.202300245
- [55] Wu LZ, Lin CH, Ma XJ, et al. Reliably characterizing the performance of thermoelectric coolers. *Rev Sci Instrum.* (2026);97(1):015205. doi: 10.1063/5.0305512

Figures:

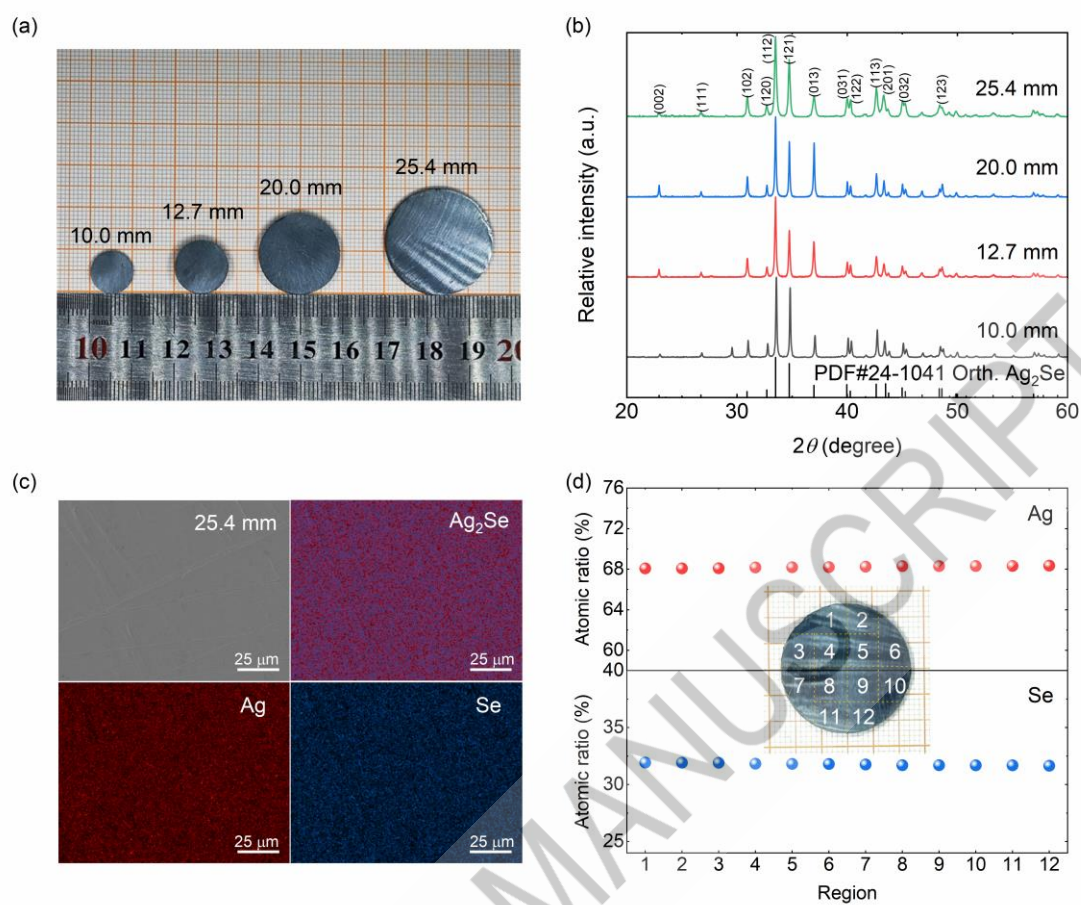


Figure 1. Phase structure and compositional homogeneity of the prepared Ag_2Se sample. (a) Optic images and (b) XRD patterns of Ag_2Se samples with different sizes. (c) Surface morphology and elemental distribution, and (d) EPMA results of the $\phi 25.4$ Ag_2Se sample.

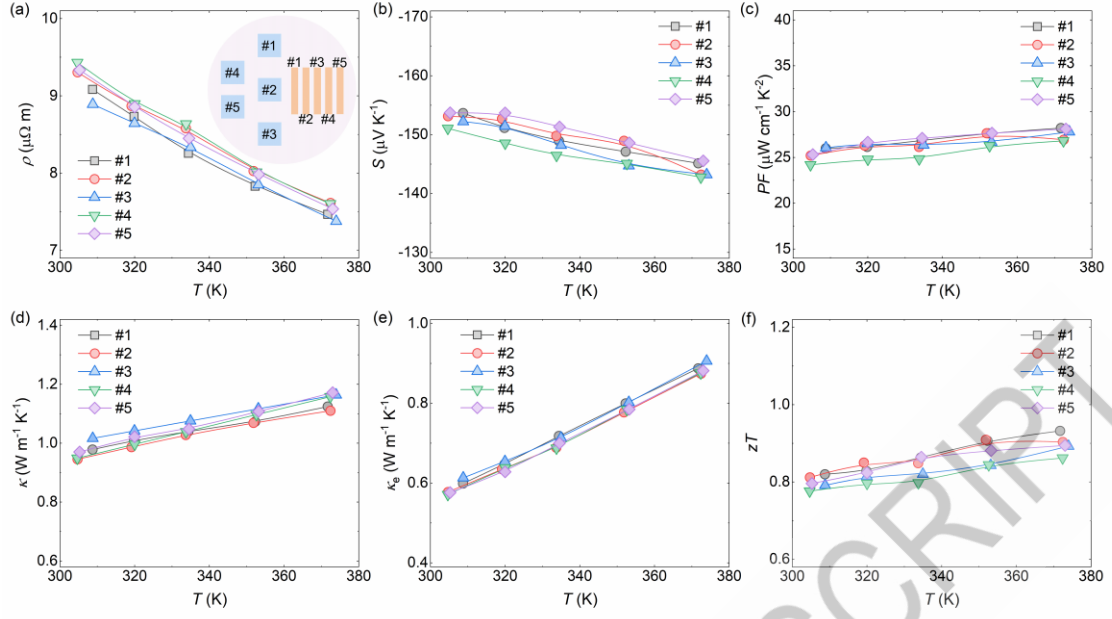


Figure 2. Thermoelectric properties of the $\phi 25.4$ Ag_2Se samples. Temperature-dependent (a) electrical resistivity, (b) Seebeck coefficient, (c) power factor, (d) thermal conductivity, (e) the sum of electronic and bipolar thermal conductivity, and (f) zT values.

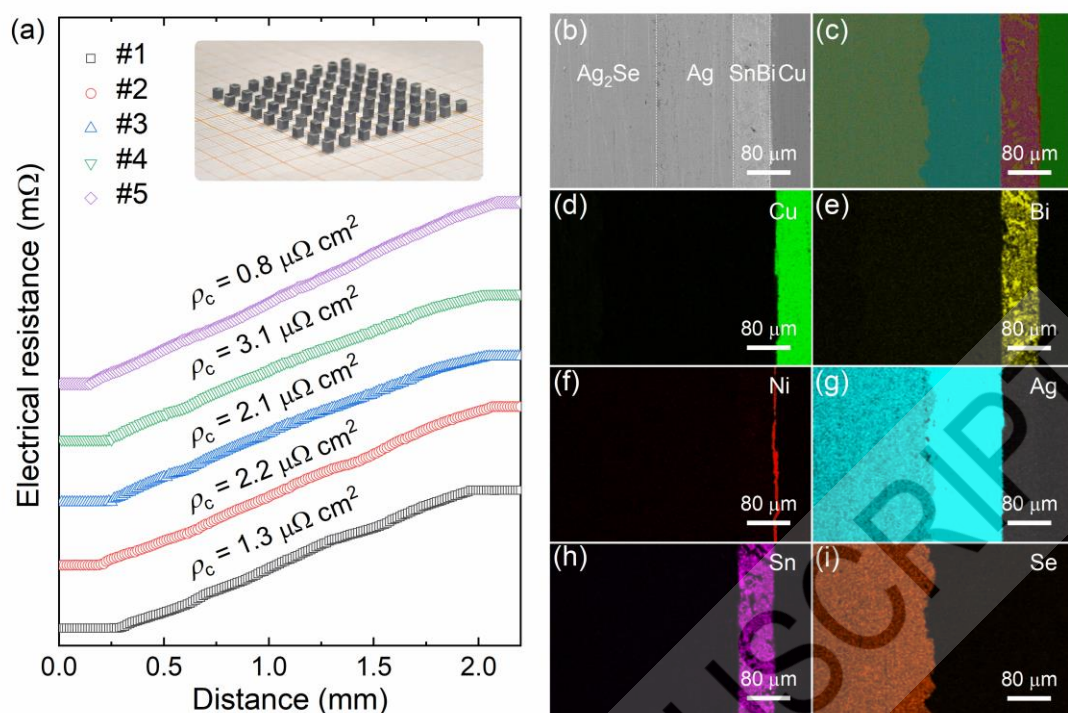


Figure 3. Interfacial properties of Ag₂Se-based interface. (a) Contact resistivity for five Ag/Ag₂Se/Ag legs. The inset shows the prepared Ag/Ag₂Se/Ag legs. (b) The interface of the soldered Ag₂Se leg joint and (c-i) their corresponding EDS mapping for the interface.

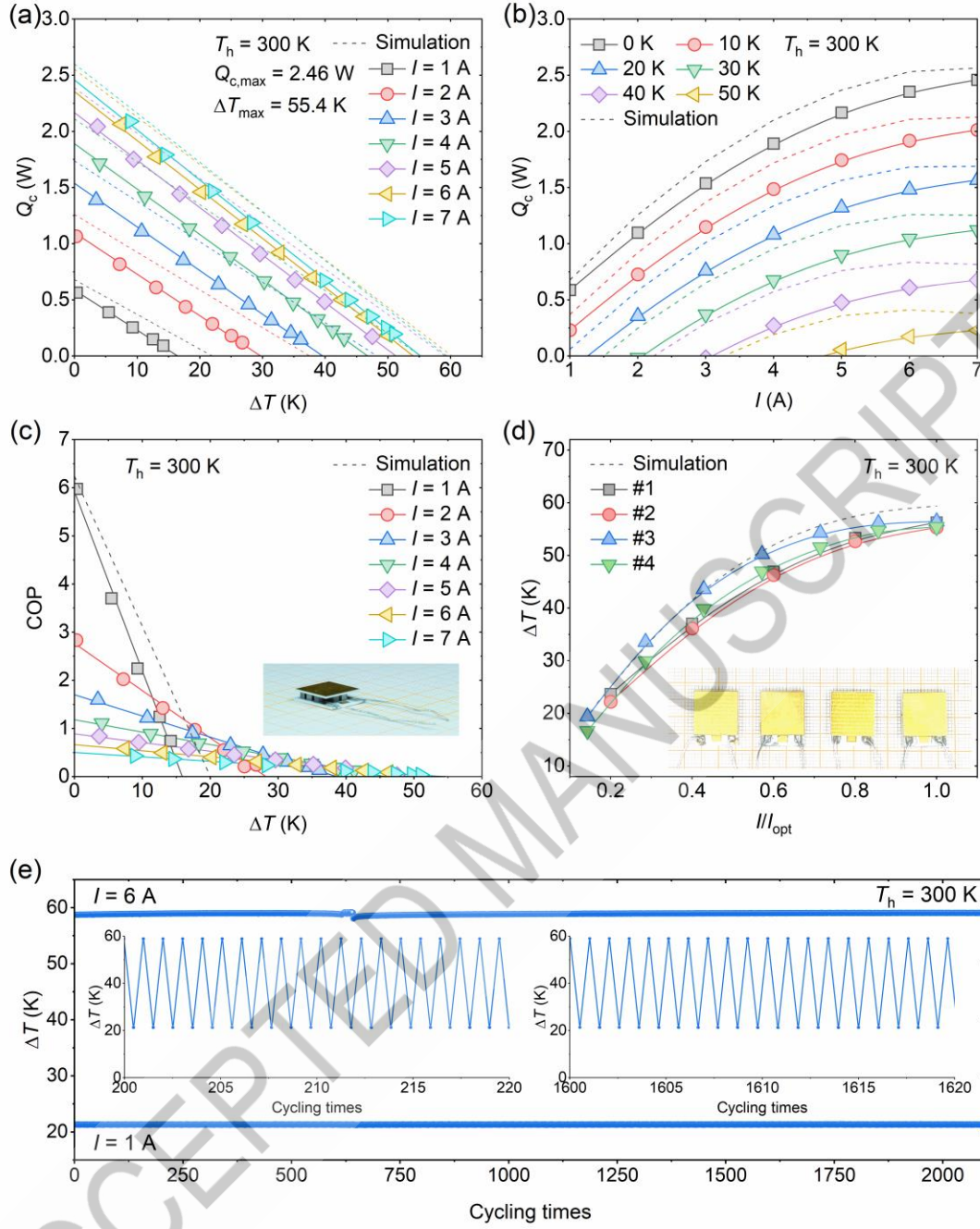


Figure 4. Thermoelectric cooling performance of Ag₂Se-based device at the hot-side temperature of 300 K. Cooling power as a function of (a) cooling temperature difference at varying electrical currents and (b) electrical current at varying cooling temperature differences. (c) Coefficient of performance as a function of cooling temperature difference. (d) The relationship between cooling temperature difference and electrical currents for four Ag₂Se-based coolers. (e) Cycling of the Ag₂Se-based thermoelectric cooler for more than 2000 times between 1 A and 6 A. The insets present the cycling test data.

Supplementary information

Towards the practical realization of high-performance Ag₂Se-based thermoelectric coolers

Feng Jiang^{a†}, Zhengtao Wang^{a†}, Wen Zhong^a, Yifan Zhou^a, Zhengyang Zhou^a, Longzhi Wu^a, Jiang Chen^a, Yao Xu^a, Xiaodong Wang^{a,d}, Feng Cao^c, Qian Zhang^{a, b, e*}, and Jun Mao^{a, b, e*}

a School of Materials Science and Engineering, and Institute of Materials Genome & Big Data, Harbin Institute of Technology (Shenzhen), Shenzhen 518055, P.R. China.

b State Key Laboratory of Precision Welding & Joining of Materials and Structures, Harbin Institute of Technology, Harbin 150001, P.R. China.

c School of Science, Harbin Institute of Technology (Shenzhen), Shenzhen 518055, P.R. China.

d Institute of Special Environments Physical Sciences, Harbin Institute of Technology (Shenzhen), Shenzhen 518055, P.R. China.

e School of Materials Science and Engineering, Shenzhen Key Laboratory of New Materials Technology, Shenzhen 518055, P.R. China.

[†]These authors contributed equally to this work.

*Corresponding authors, email: zhangqf@hit.edu.cn; maojun@hit.edu.cn;

Contents

1. Setting parameters for the finite element simulation of Ag₂Se-based cooler
2. Sample density of Ag₂Se materials with different sizes
3. Specific heat capacity of the Ag₂Se sample
4. Energy dispersive spectroscopy mapping of the Ag₂Se sample
5. Hall carrier concentration and mobility of the Ag₂Se sample
6. The lattice thermal conductivity of the Ag₂Se sample
7. Thermoelectric properties of five Ag₂Se samples
8. Contact resistivity of the soldered Ag/Ag₂Se joint
9. Energy dispersive spectroscopy and linear scanning of the Ag/Ag₂Se interface
10. Linear energy dispersive spectroscopy scanning of the Ag/SnBi interface
11. Comparison of thermoelectric cooling performance for Ag₂Se, Bi₂Te₃, and Mg₃(Sb, Bi)₂-based devices at the hot-side temperature of 300 K
12. The simulated cooling performance of the 7 pairs Ag₂Se/(Bi, Sb)₂Te₃ thermoelectric cooler
13. Thermoelectric cooling performance of the Ag₂Se-based cooler at the hot-side temperature of 325 K
14. Coefficient of performance as a function of the electrical current of the Ag₂Se-based thermoelectric cooler
15. Interfacial properties of the Ag₂Se-based thermoelectric cooler after cycling

1. Setting parameters for the finite element simulation of Ag₂Se-based cooler

Table S1. Finite element simulation setting parameters.

Parameter	Value
Cross-sectional area of the Ag ₂ Se legs	$1.8 \times 1.8 \text{ mm}^2$
Height of the Ag ₂ Se legs	2.5 mm
Cross-sectional area of the (Bi, Sb) ₂ Te ₃ legs	$2.0 \times 2.0 \text{ mm}^2$
Height of the (Bi, Sb) ₂ Te ₃ legs	2.5 mm
Thickness of copper electrode	0.065 mm
Thickness of Al ₂ O ₃ substrate	0.38 mm
The area of the Al ₂ O ₃ substrate of the cold side	$13.0 \times 13.0 \text{ mm}^2$
The area of the Al ₂ O ₃ substrate of the hot side	$13.0 \times 16.0 \text{ mm}^2$
Thermal conductivity of the substrate	$20 \text{ W m}^{-1} \text{ K}^{-1}$
Thermal conductivity of the thermal grease	$4.8 \text{ W m}^{-1} \text{ K}^{-1}$
Heat load	0.0-2.5 W
Hot-side temperature	300 K
Contact resistivity of Ag ₂ Se legs	$5.0 \mu\Omega \text{ cm}^2$
Contact resistivity of (Bi, Sb) ₂ Te ₃ legs	$5.0 \mu\Omega \text{ cm}^2$

2. Sample density of Ag₂Se materials with different sizes

Table S2. Sample density of Ag₂Se materials with different sizes

Sample diameter (mm)	Measured density (g cm ⁻³)	Relative density (%)
10.0	8.05	98.17
12.7	8.07	98.41
20.0	8.03	97.93
25.4	8.06	98.29

3. Specific heat capacity of the Ag₂Se sample

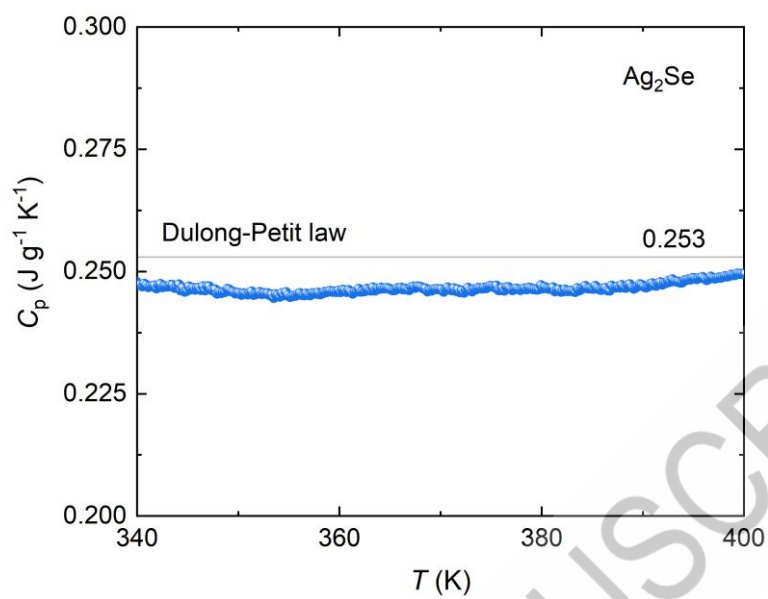


Figure S1. Specific heat capacity of the Ag₂Se sample.

4. Energy dispersive spectroscopy mapping of the Ag_2Se sample

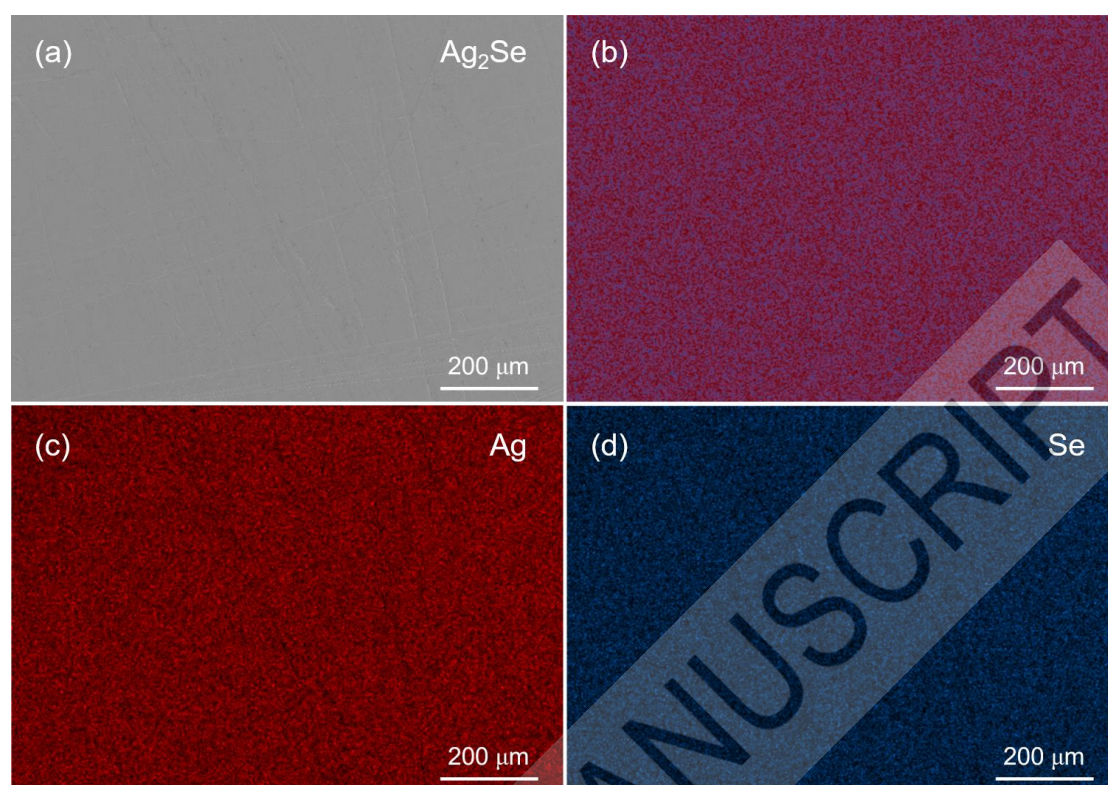


Figure S2. (a) Surface morphology, and (b-d) energy dispersive spectroscopy mapping of the Ag_2Se sample.

5. Hall carrier concentration and mobility of the Ag₂Se sample

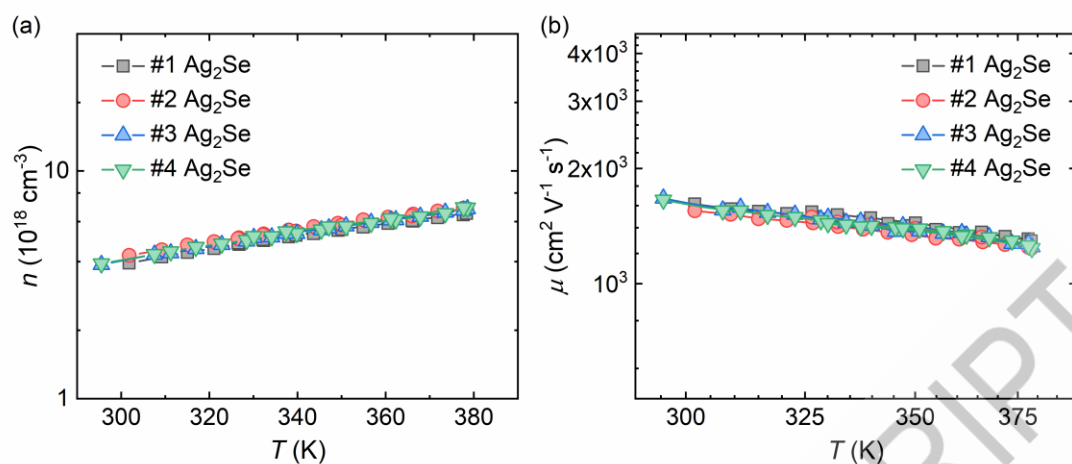


Figure S3. Hall carrier concentration and mobility of the Ag₂Se sample. (a) Carrier concentration. (b) Carrier mobility.

6. The lattice thermal conductivity of the Ag₂Se sample

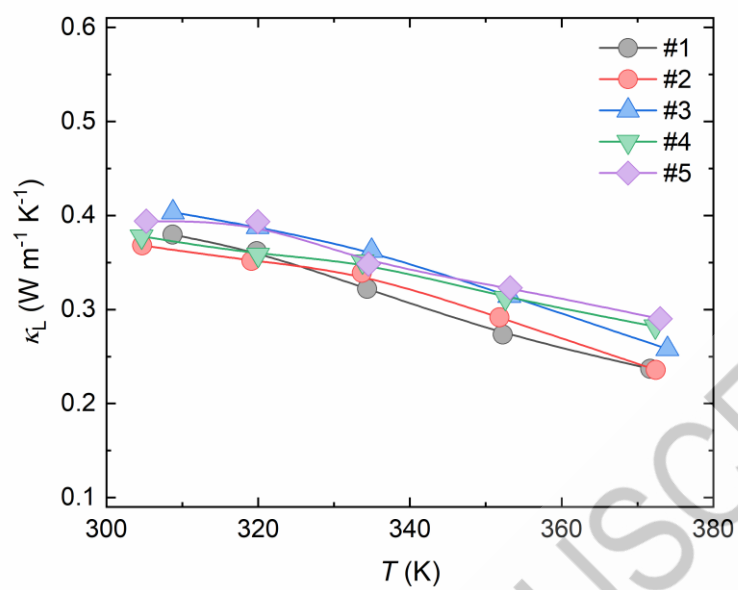


Figure S4. The lattice thermal conductivity of the Ag₂Se sample.

7. Thermoelectric properties of the Ag₂Se samples

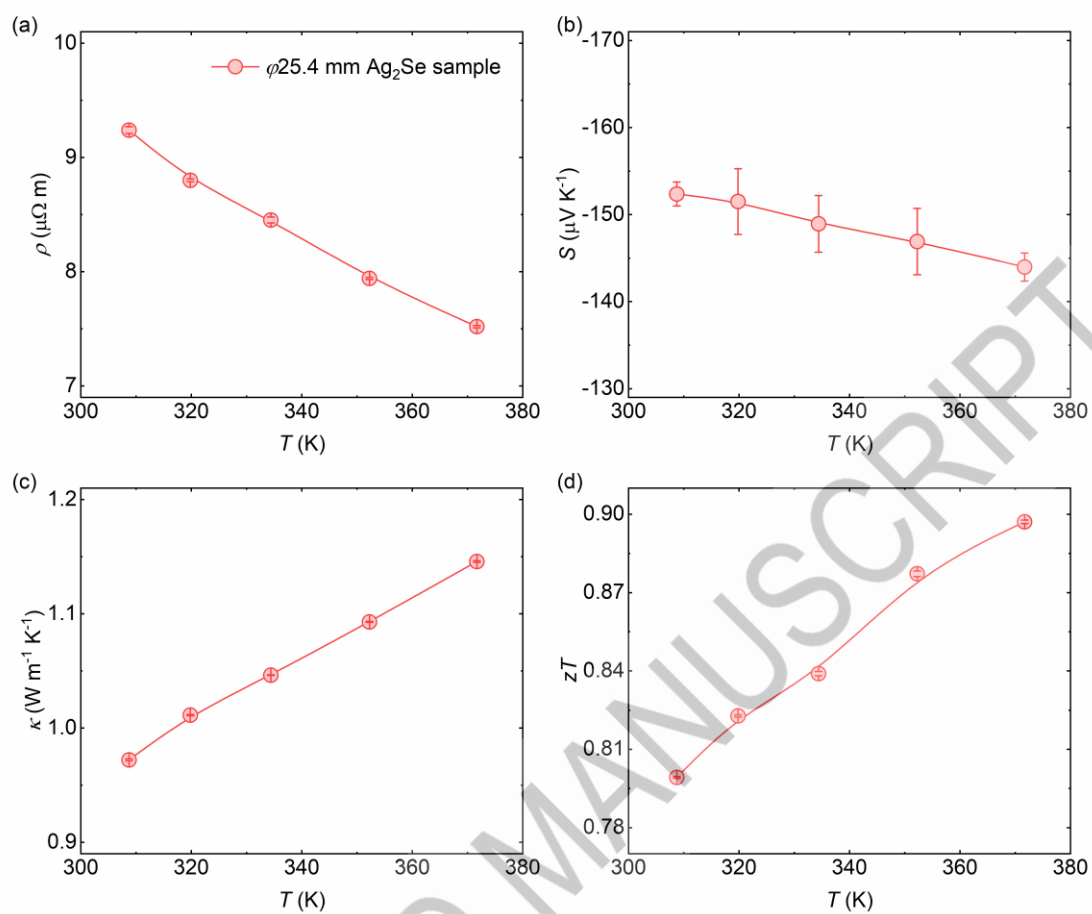


Figure S5. Thermoelectric properties of the Ag₂Se samples. Temperature-dependent (a) electrical resistivity, (b) Seebeck coefficient, (c) thermal conductivity, and (d) zT values.

8. Contact resistivity of the soldered Ag/Ag₂Se joint

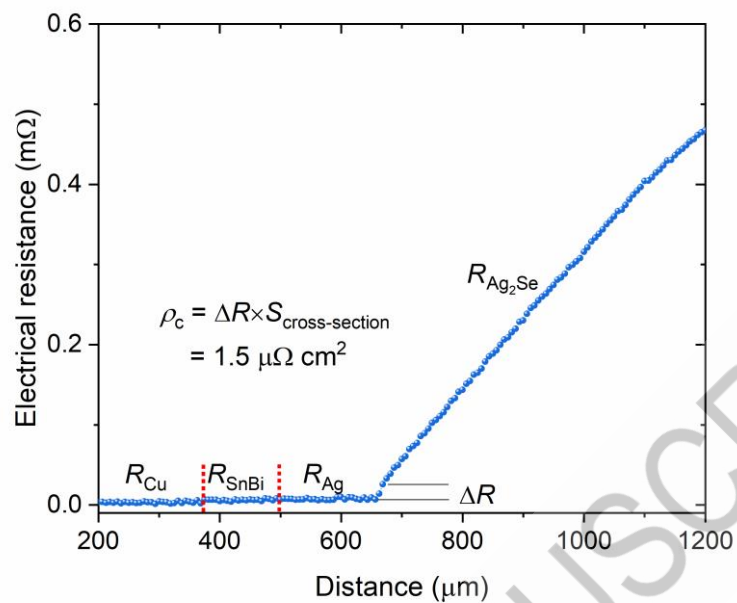


Figure S6. Contact resistivity of the soldered Ag/Ag₂Se joint.

9. Energy dispersive spectroscopy and linear scanning of the Ag/Ag₂Se interface

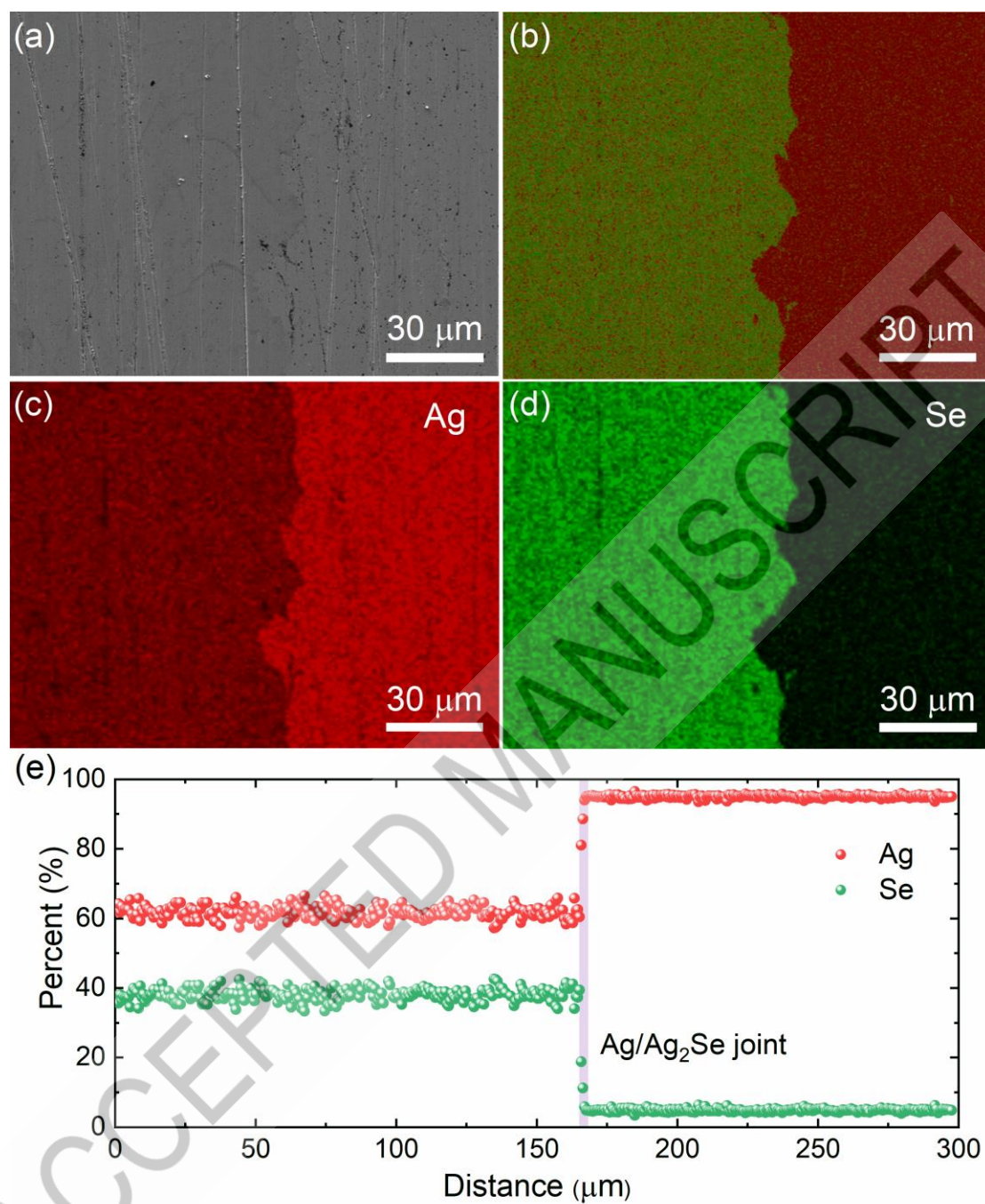


Figure S7. (a) The Ag/Ag₂Se interface and (b-d) corresponding EDS mapping for the interface. (e) Linear EDS scanning across the Ag/Ag₂Se interface.

10. Linear energy dispersive spectroscopy scanning of the Ag/SnBi interface

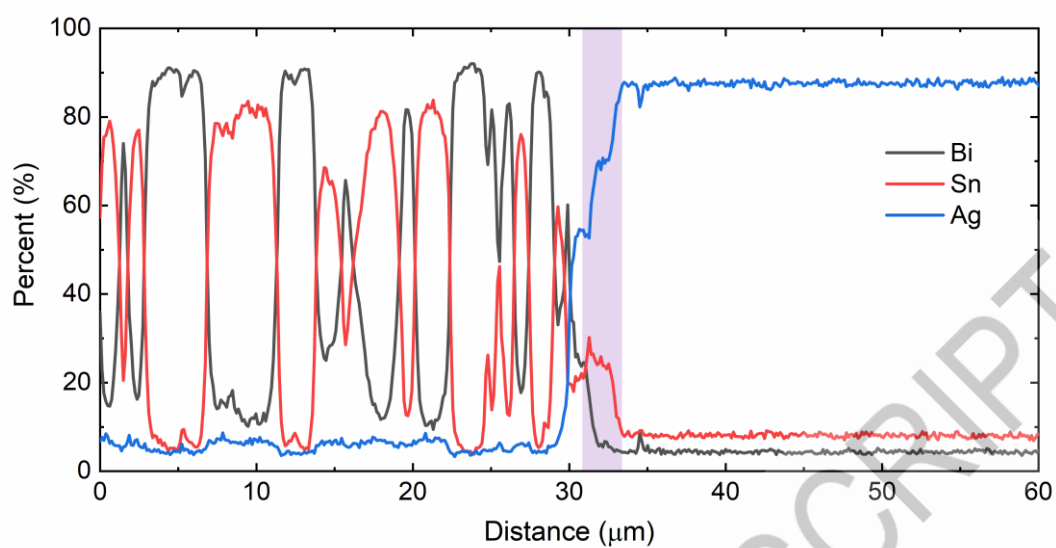


Figure S8. Linear EDS scanning across the Ag/SnBi solder interface.

11. Comparison of thermoelectric cooling performance for Ag₂Se, Bi₂Te₃, and Mg₃(Sb, Bi)₂-based devices at the hot-side temperature of 300 K

Table S3. Comparison of thermoelectric cooling performance for Ag₂Se, Bi₂Te₃, and Mg₃(Sb, Bi)₂-based devices at the hot-side temperature of 300 K

n-type leg	p-type leg	Cooling temperature difference (K)	Cooling power density (W cm ⁻²)	Reference
Ag ₂ Se	Bi ₂ Te ₃ alloys	55.4	1.5	This work
Ag ₂ Se	Bi ₂ Te ₃ alloys	57.7	1.5	Jiang <i>et al.</i> ^[1]
Ag ₂ Se	Bi ₂ Te ₃ alloys	56.0	1.4	Liu <i>et al.</i> ^[2]
Ag ₂ Se	MgAgSb	52.0	0.8	Zhao <i>et al.</i> ^[3]
Bi ₂ Te ₃	Bi ₂ Te ₃ alloys	70.1	1.6	Sun <i>et al.</i> ^[4]
Bi ₂ Te ₃	Bi ₂ Te ₃ alloys	73.9	2.2	Zhao <i>et al.</i> ^[5]
Mg ₃ (Sb, Bi) ₂	Bi ₂ Te ₃ alloys	69.0	1.3	Ma <i>et al.</i> ^[6]
Mg ₃ (Sb, Bi) ₂	MgAgSb	52.0	0.8	Xie <i>et al.</i> ^[7]
Mg ₃ (Sb, Bi) ₂	MgAgSb	61.0	-	Zhang <i>et al.</i> ^[8]

12. The simulated cooling performance of the 7 pairs $\text{Ag}_2\text{Se}/(\text{Bi}, \text{Sb})_2\text{Te}_3$ thermoelectric cooler

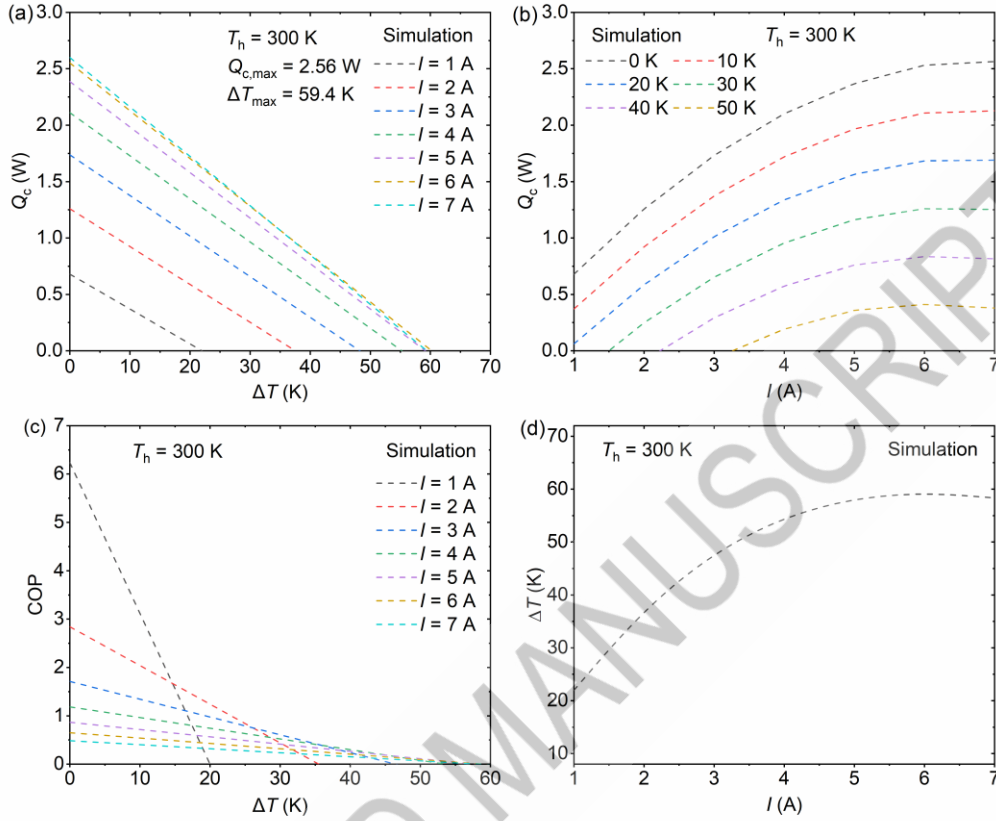


Figure S9. The simulated cooling performance of the 7 pairs $\text{Ag}_2\text{Se}/(\text{Bi}, \text{Sb})_2\text{Te}_3$ thermoelectric cooler. Cooling power as a function of (a) the temperature difference at different electrical currents and (b) electrical current at different temperature differences. (c) The coefficient of performance as a function of the temperature difference at different electrical currents. (d) The maximum cooling temperature difference at different electrical currents.

13. Thermoelectric cooling performance of the Ag₂Se-based cooler at the hot-side temperature of 325 K

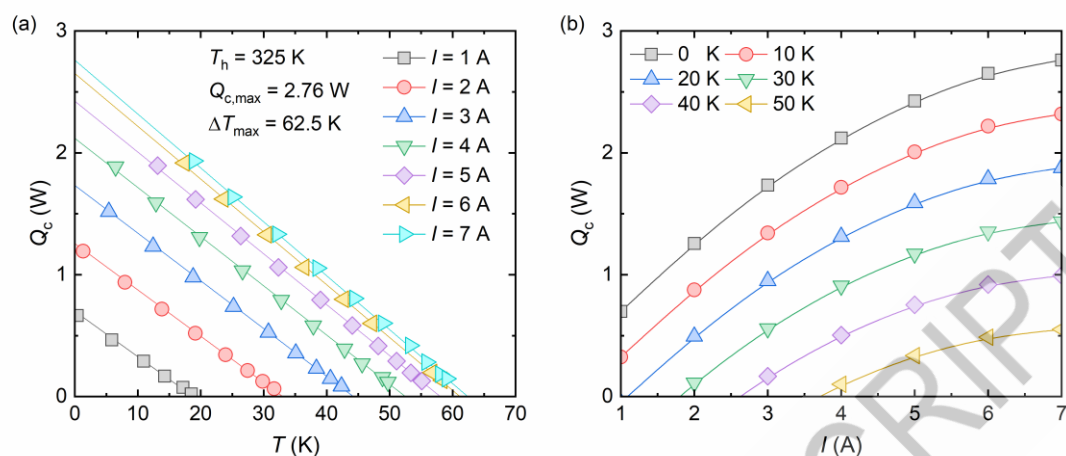


Figure S10. Cooling power as a function of (a) cooling temperature difference at different electrical currents, and (b) electrical current at different cooling temperature differences.

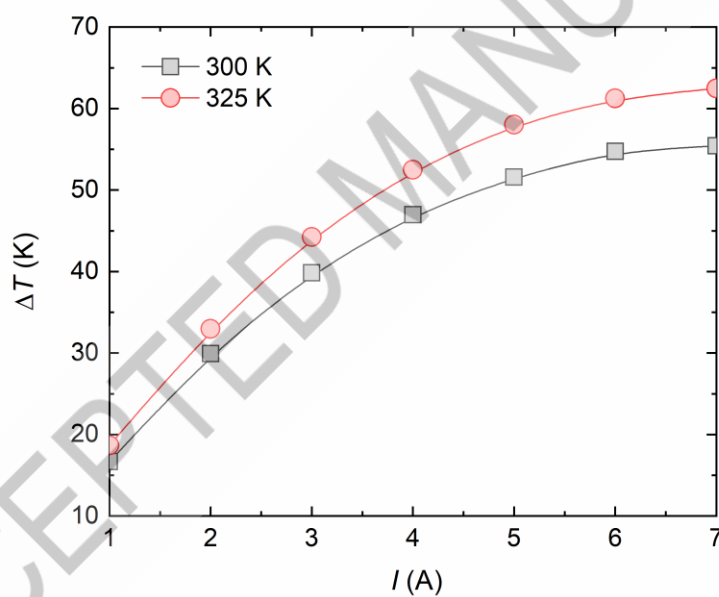


Figure S11. The relationship between cooling temperature difference and electrical current at the hot-side temperature of 300 and 325 K.

14. Coefficient of performance as a function of the electrical current of the Ag_2Se -based thermoelectric cooler

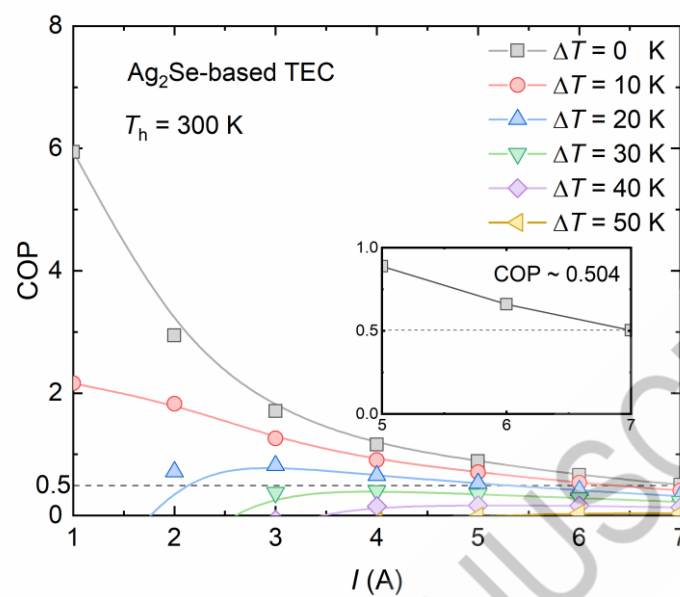


Figure S12. Coefficient of performance as a function of the electrical current of the Ag_2Se -based thermoelectric cooler at the hot-side temperature of 300 K.

15. Interfacial properties of the Ag₂Se-based thermoelectric cooler after cycling

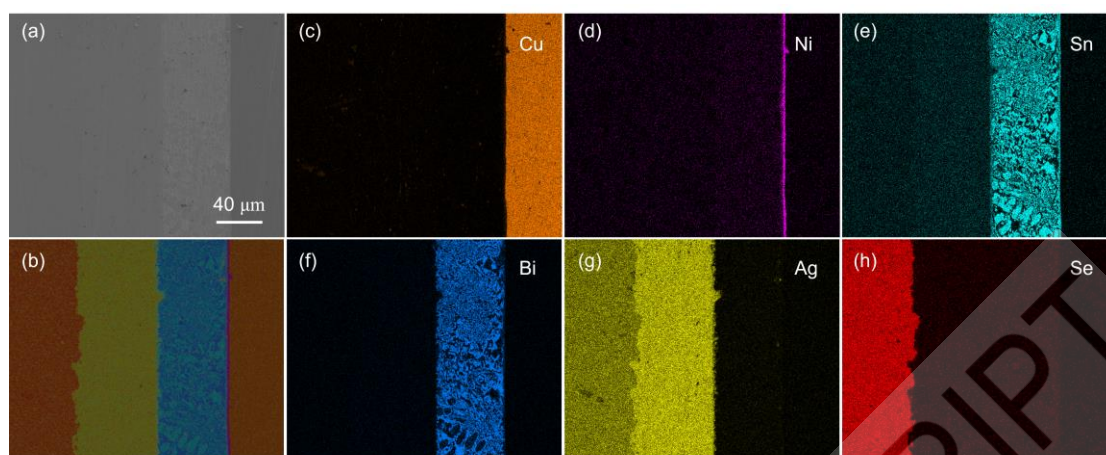


Figure S13. (a) Interfacial morphology, and (b-h) energy dispersive spectroscopy mapping of the interface of the Ag₂Se-based thermoelectric cooler.

References:

- [1] Jiang F, Lin CH, Cheng JX, et al. Prefer-oriented Ag₂Se crystal for high-performance thermoelectric cooling. *Adv Funct Mater.* (2024);35(6):2415000. doi: 10.1002/adfm.202415000
- [2] Liu M, Zhang XY, Zhang SX, et al. Ag₂Se as a tougher alternative to n-type Bi₂Te₃ thermoelectrics. *Nat Commun.* (2024);15(1):6580. doi: 10.1038/s41467-024-50898-6
- [3] Zhao SY, Shi XL, Zhou Q, et al. Substitution energy-guided screening of diffusion barrier materials for Ag₂Se-based thermoelectric coolers. *Nano Res.* (2025);18(10):94907903. doi: 10.26599/NR.2025.94907903
- [4] Sun YX, Wu H, Dong XY, et al. High performance BiSbTe alloy for superior thermoelectric cooling. *Adv Funct Mater.* (2023);33(28):2301423. doi: 10.1002/adfm.202301423
- [5] Zhang Y, Xu G, Nozariasbmarz A, et al. Thermoelectric cooling performance enhancement in BiSeTe alloy by microstructure modulation via hot extrusion. *Small Sci.* (2023);4(2):2300245. doi: 10.1002/smssc.202300245
- [6] Ma XJ, Lin CH, Yang HY, et al. Elevating thermoelectric performance in the sub-ambient temperature range for electronic refrigeration. *Innovation.* (2025);6(5):100864. doi: 10.1016/j.xinn.2025.100864
- [7] Xie LJ, Yang JW, Liu ZY, et al. Highly efficient thermoelectric cooling performance of ultrafine-grained and nanoporous materials. *Mater Today.* (2023);65(4):5-13. doi: 10.1016/j.mattod.2023.03.021
- [8] Zhang XF, Zhu HT, Dong XJ, et al. High-performance MgAgSb/Mg₃(Sb,Bi)₂-based thermoelectrics with $\eta = 12\%$ at $T \leq 583\text{K}$. *Joule.* (2024);8(12):3324-3335. doi: 10.1016/j.joule.2024.08.013

Graphical Abstract

